AVO analysis for a single thin bed using three-layer media equation

Wenyong Pan

ABSTRACT

As effective criteria for hydrocarbon detection, Amplitude Versus Offset (AVO) technology has been widely used in the recent years. Zoeppritz equation, which describes the reflection and transmission of plane wave on a single interface separating two half infinite spaces, is the basis for traditional AVO analysis. This characteristic of Zoeppritz equation makes it unsuitable to analyze the propagation of wave in multi-layered media when the layers are very thin. This study derives the three-layer media equation based on multi-layer media equation by Breshkovsky in elastic regime for discussing the reflection and transmission of plane wave in thin bed. For that the reflection coefficient is a continuous function of incident angle, frequency and thin bed thickness, it is possible to analyze the AVO effects with varying the incident angle, frequency and thin layer thickness. It is concluded that (1) three-layer media equation is more quantitative and precise than Zoeppritz equation to analyze the AVO responses of thin bed; (2) the influence of thin bed thinning on variations of amplitudes is equal to that of dominant frequency decreasing; (3) AVO analysis of P-S wave helps us to eliminate the problem of multi-solutions in fluids prediction; (4) With decreasing Q (quality factor), the AVO curve obtained from three-layer media equation become more smooth and get closer to the curve calculated by Zoeppritz equation.

INTRODUCTION

Amplitude Versus Offset (AVO) or Amplitude Versus Angle (AVA) analyses are using the variation information of pre-stack amplitude to reflect the variation characteristics of rock and fluid in reservoir. In the exploration industry, AVO analysis is particularly suitable for the detection and mapping of gas zones since reservoirs often consist of shale with high Poisson's ratio (highV_p/V_s) overlying gas bearing sands with low Poisson's ratio (lowV_p/V_s) (Juhlin and Young, 1993). The basis for traditional AVO analysis is Zoeppritz equation derived by Zoeppritz (1919), which describes how transmission and reflection coefficients vary with angle for plane wave impinging upon a single interface separating two half infinite spaces. Many scientists (Koefoed, 1955; Aki and Richards, 1980; Shuey, 1985; Gidlow et al., 1992; Inannen, 2011) made great efforts to facilitate its application by deriving the linear approximations of Zoeppritz equation.

However, with the further development of seismic exploration, Zoeppritz equation shows its disadvantages in quantitative interpretation of thin bed. As the layer thinning, the reflections from the top and bottom interfaces interfere or stack, which are significantly different from the reflections on a single interface. The problems associated with thin bed interested scientists early. Widess (1973) studied the reflections at the top and bottom interfaces of a thin layer at normal incidence when a thin layer was inter-bedded in a homogeneous background. He also found that the maximum constructive

interference for a zero-phase wavelet occurred when the bed thickness was one-quarter of the dominant wavelength-"tuning thickness". In the later years, the scientists did a lot of researches on the AVO effects of thin bed with varying the thin bed thickness. For exploration geophysics, the generally accepted threshold for vertical resolution of a layer is a quarter of the dominant wavelength (Liu and Schmitt, 2003). In this paper, the layer is called a thin layer when$1 \leq \mathrm{n} = \lambda/d < 4$, and an ultra-thin layer when$4 \leq \lambda/d$, where λ and d are the dominant wavelength the thickness of Layer 2 respectively. (Liu and Schmitt, 2003). Swan (1988) analyzed the AVO responses in a finely layered medium and found that AVO distortions due to tuning may be larger than the underlying lithological AVO effect. Ball (1988) extended the traditional zero-offset tuning analysis by the additional information in offset domain. Chung and Lawton (1995) developed expressions for the normal incidence amplitude response of a thin layer for the general case of unequal reflection coefficients at the top and bottom of the bed. Liu and Schmitt (2003) derived an exact analytical solution to model the reflection amplitude and amplitude variation with offset (AVO) responses of a single thin bed for arbitrary incident angles in acoustic regime.

These researches carried out by the above scientists are either based on ray theory or at normal incidence or in acoustic regime. In this study, the three-layer media equation based on multi-layer media equation (Breshkovsky, 1960) is derived to study the AVO responses of thin bed with the variations of incident angle, frequency, and thin bed thickness with attenuation and no attenuation, comparing with that derived from Zoeppritz equation. Several conclusions are arrived at:

(1) Comparing with the AVO curves calculated by Zoeppritz equation, the AVO curves of thin bed calculated by three-layer media equation, taking the reflections from the bottom interface into account, are more quantitative and precise.

(2) At fixed incidence (0° -30°), for ultra-thin layer ($4 \leq \lambda/d$), with the target thin bed thinning, the absolute reflection coefficients become smaller. And when$4 = \lambda/d$, the absolute reflection coefficient is the biggest;

(3) For fixed thickness of ultra-thin bed ($4 \leq \lambda/d$), with increasing incident angle, the absolute reflection coefficients become smaller when rock type of target layer is water sand for Model I. While the absolute reflection coefficients become bigger when rock type of target layer is gas sand;

(4) With increasing the incident angle, the amplitude anomaly obtained by three-layer equation may be different from the amplitude anomaly obtained by Zoeppritz equation;

(5) The influence of thin bed thinning on variations of amplitudes is equal to that of dominant frequency decreasing;

(6) AVO analysis of P-S wave helps us settle the problem of multi-solutions in hydrocarbon detection;

(7) With the thin bed thinning, the differences of reflection coefficients become smaller for different P-velocities of Layer 2 at small incidence (0° -30°);

(8) With decreasing Q (quality factor), the AVO curve calculated by three-layer media equation become more smooth and get closer to the curve calculated by Zoeppritz equation.

Theory and Algorithm

Model

Figure 1 show the three-layer model used in this research. The target layer (Layer 2 shown in Figure 1) is embedded between two infinite half spaces. And a plane harmonic and compressional wave illuminates on Interface 1, which causes the reflected compressional wave (P-wave) and shear wave (only SV-wave is considered here), transmitted compressional wave and shear wave. The transmitted P-wave and S-wave (SV-wave) cause reflection and transmission on Interface 1 and Interface 2 again and produce multi-reflections within Layer 2.

The parameters of the models are listed in Table 1. Model I consist of shale overlying water sand or gas sand in mid-depth layer (9000ft or 2743m in depth) whereas Model II is in shallow layer (4000ft or 1219m in depth) with shale overlying water sand, gas sand or coal (Hilterman, 2001). At normal incidence, for Model I, when Layer 2 is water sand, the reflection is positive for that the impedance of Layer 2 is smaller than that of Layer 1 (shale). While when the water sand is replaced by gas sand, the reflection changes to negative. This “polarity conversion” anomaly helps us to recognize gas reservoir. For Model II, the polarities of the reflections are identical for water sand, gas sand or coal within Layer 2. While the replacement of gas sand or coal within Layer 2 cause the increase of absolute amplitudes which is called “bright spot” anomaly. In this study, we analyze the AVO/AVA responses of target Layer 2 for Model I with varying incident angle, thickness of the target layer, and dominant frequency. While Model II is an example to analyze the AVO response of P-SV wave which can help us to predict the hydrocarbon more precisely.

What’s more, the influences of quality factor (Q), which describes the energy attenuation of seismic wave within the medias (only the target Layer 2 is considered here), are also discussed in this paper.

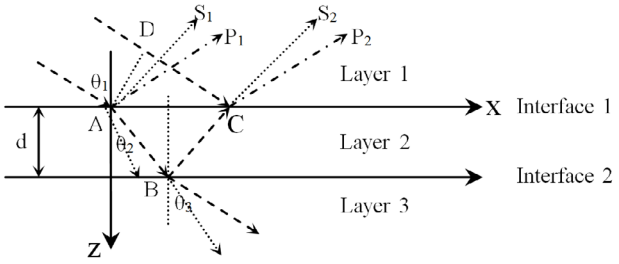

FIG.1. Three-layer media model $\Delta t = T_{ABC} - T_{DC} = 2d\cos\theta_2/\alpha_2$

Table 1. Elastic Parameters of Model I and Model II (Hilterman, 2001)

Model	Rock type	α (m/s)	β (m/s)	α/β	ρ (g/cm^3)	σ
Model I	Shale	2642.6	1166.7	2.23	2.29	0.38
	Water sand	3048.0	1525.0	1.91	2.23	0.31
	Gas sand	2781.3	1664.8	1.67	2.08	0.22
	Shale	2642.6	1166.7	2.23	2.29	0.38
Model II	Shale	2191.5	818.0	2.67	2.16	0.42
	Water sand	2133.6	859.0	2.48	2.11	0.40
	Gas sand	1542.6	900.0	1.71	1.88	0.24
	Coal	1400.0	700.0	2.00	1.40	0.33
	Shale	2191.5	818.0	2.67	2.16	0.42

Method

Breshkovsky (1960) analyzed the propagation of plane wave in multi-layered and elastic media and built the multi-layered media equation. This equation connects the displacement of stress of top layer and bottom layer through one coefficients matrix as shown in equation (1).

$$\begin{bmatrix} u_x{}^n \\ v_z{}^n \\ \sigma_{zz}{}^n \\ \tau_{zx}{}^n \end{bmatrix} = \begin{bmatrix} A_{11} & A_{12} & A_{13} & A_{14} \\ A_{21} & A_{22} & A_{23} & A_{24} \\ A_{31} & A_{32} & A_{33} & A_{34} \\ A_{41} & A_{42} & Ac_{34} & A_{44} \end{bmatrix} \begin{bmatrix} u_x{}^1 \\ v_z{}^1 \\ \sigma_{zz}{}^1 \\ \tau_{zx}{}^1 \end{bmatrix}, \quad (1)$$

where $u_x{}^n$, $v_z{}^n$, $\sigma_{zz}{}^n$, $\tau_{zx}{}^n$, $u_x{}^1$, $v_z{}^1$, $\sigma_{zz}{}^1$, and $\tau_{zx}{}^n$ represent the displacements and stresses in Layer n and Layer 1. Here in this study, the multi-layer media model is simplified to three-layer media model (as shown in Figure 1) in which the parameters of Layer 1 are equal to those of Layer 2 for computational convenience. The three-layer

media equation is also derived (equation (2)). The deriving process is shown in Appendix A.

$$\begin{bmatrix} {u_x}^3 \\ {v_z}^3 \\ {\sigma_{zz}}^3 \\ {\tau_{zx}}^3 \end{bmatrix} = \begin{bmatrix} c_{11} & c_{12} & c_{13} & c_{14} \\ c_{21} & c_{22} & c_{23} & c_{24} \\ c_{31} & c_{32} & c_{33} & c_{34} \\ c_{41} & c_{42} & c_{34} & c_{44} \end{bmatrix} \begin{bmatrix} {u_x}^1 \\ {v_z}^1 \\ {\sigma_{zz}}^1 \\ {\tau_{zx}}^1 \end{bmatrix}, \tag{2}$$

Then we can get the reflection and transmission coefficients which are the functions of incident angle θ, dominant frequency f and target thin layer thickness d. It is easier for us to study the influences of frequency and thin layer thickness to amplitudes comparing with Zoeppritz equation.

$$R_{pp}(\theta, f, d) = \frac{\det V_{pp}}{\det V}, R_{ps}(\theta, f, d) = \frac{\det V_{ps}}{\det V}, T_{pp}(\theta, f, d) = \frac{\det V'_{pp}}{\det V}, T_{ps}(\theta, f, d) = \frac{\det V'_{ps}}{\det V}$$

Even though, we don't derive the direct expression of reflection coefficient or its linear approximations. We can still analyze the variations of amplitudes with varying incident angle, frequency and thin bed thickness in elastic regime. The equation is too complicated to inverse directly. We can get the inversion results by non-linear optimization algorithms such as Simulated Annealing Algorithm or Genetic Algorithm.

Liu and Schmitt (2003) derived the reflection coefficients equation for thin bed in acoustic regime which can be written as

$$R(\omega) = \frac{j({Z^2}_2 - {Z^2}_1)\sin\left(\left(\frac{\omega}{\alpha_2}\right)cos\theta_2 d\right)}{j({Z^2}_2 + {Z^2}_1)\sin\left(\left(\frac{\omega}{\alpha_2}\right)cos\theta_2 d\right) + 2Z_1 Z_2 \cos\left(\left(\frac{\omega}{\alpha_2}\right)cos\theta_2 d\right)}, \tag{3}$$

So, by comparing the AVO response obtained by three-layer equation with that obtained by Liu and Schmitt's equation for Model II, we discuss the importance and usefulness of P-SV wave AVO analysis which makes the hydrocarbon prediction more precise.

According to the theory of internal friction, the energy of seismic wave attenuates when propagating within the medium. And Frayer (1978) gave the relationship of velocity and quality factor Q which describes the relative energy change in the domain of one wave length.

$$\frac{1}{Q} = \frac{1}{2\pi}\frac{\Delta E}{E} = \frac{(k^2)_I}{(k^2)_R}, \tag{4}$$

where E and k are the energy and complex wave-number. And $(k^2)_I$ and $(k^2)_R$ represent the imaginary part and real part ofk^2. And

$$k = \frac{\omega}{V} = \frac{\omega}{V_R + jV_I}, \tag{5}$$

Substituting equation (4) into equation (3) and we can get

$$V \approx V_R + j\left(\frac{V_R}{2Q}\right), \quad (6)$$

Substituting the P-wave velocity and S-wave velocity in R_{pp}, R_{ps}, T_{pp}, T_{ps} with equation (6), we can get relative reflection and transmission coefficients formulas.

AVO RESPONSES OF THIN BED WITH NO ATTENUATION

AVO responses of P-P wave with no attenuation

Figure 2 shows P-P Wave absolute reflection coefficients without attenuation for different $n = \lambda/d$ (n=1, 2, 4, 6, 8, 10, 20) for Model I with water sand (a) and gas sand (b) in Layer 2 at full angles. The dashed line is calculated by Zoeppritz equation and other lines are calculated by three-layer media equation. It can be seen that reflection coefficients curves calculated by three-layer media equation are quite different from that calculated by Zoeppritz equation especially for post-critical incidence.

We can analyze the AVO responses of gas sand within Layer 2 through Figure 2 (b). And it shows that when Layer 2 is an ultra-thin layer ($n = \lambda/d \geq 4$), the absolute reflection coefficients increase slowly to a local maximum and then decrease to a local minimum and finally increase quickly to near unity. Moreover, for pre-critical angles, the bigger of$n = \lambda/d \geq 4$, the more flat the curves become, whereas for post-critical angles, the condition is opposite. When Layer 2 is a thin layer ($1 \leq n = \lambda/d < 4$), the reflection coefficients curves may have several local maximums and local minimums before critical angle (around 72°). It can be explained by ray-tracing theory and the time delay equation $\Delta t = T_{ABC} - T_{DC} = 2d\cos\theta_2/\alpha_2$ (as shown in Figure 1) in acoustic regime. For instance, when $n = \lambda/d = 1$, $\Delta t = T_{ABC} - T_{DC} = 2T\cos\theta_2$. As θ_2 increases, Δt receives $(3/2)T$ firstly when the reflections on top and bottom interfaces stack together. The incident angle θ_1 at this time is about 40° which can be calculated by Snell's law. Then Δt receives T when the reflections on top and bottom interfaces counteract with each other and θ_1 is about 55.4°. And then the reflection receive its second local maximum and second local minimum when Δt is $T/2$ and 0 and θ_1 is about 67° and 72° respectively. The degrees of incident angles calculated here are not exactly equal to the degrees shown in Figure 2 (b). This is caused by the influences of converted S-wave.

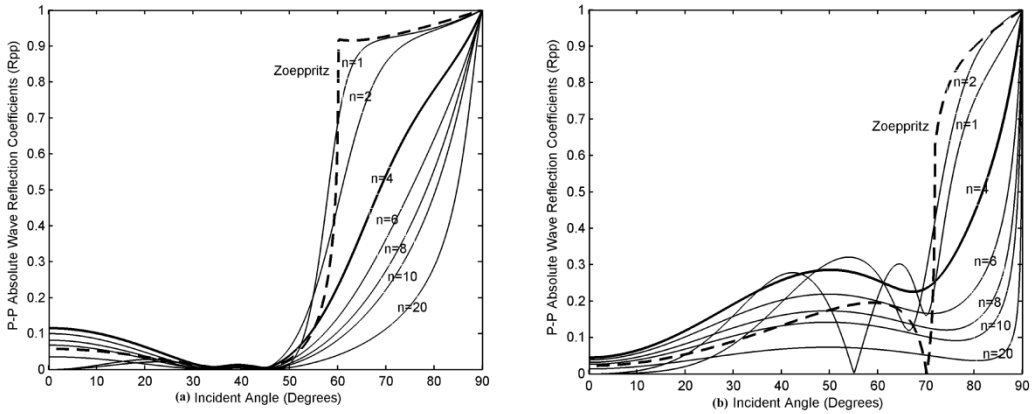

FIG.2. P-P Wave absolute reflection coefficients spectrum (frequency=30Hz) for different $n = \lambda/d$ from 1 to 20 for Model I with water sand (a) and gas sand (b) at full angles. The dashed line is calculated by Zoeppritz equation and other lines are calculated by three-layer media equation.

Figure 3 shows the absolute reflection coefficients at small incidence (from 0° to 30°) for water sand (a) and gas sand (b) in Layer 2 respectively. It can be seen that whether the target Layer 2 is water sand or gas sand, the absolute reflection coefficients, when n=4 at normal incidence (or incident angle is zero), are bigger than other absolute reflection coefficients. While when n=1 or 2, the absolute reflection coefficients are zero. This is can also explain by time delay equation. When $d = \lambda/4$ at normal incidence (without converted S wave), the time delay is $\Delta t = T_{ABC} - T_{DC} = 2d\cos\theta_2/\alpha_2 = \lambda/(2\alpha_2) = T/2$ and then the reflections from top interface and bottom interface reinforce mutually. While when $d = \lambda$ and $d = \lambda/2$ at normal incidence, the time delay is 2T and T respectively and the reflections from top interface and bottom interface weaken mutually to zero.

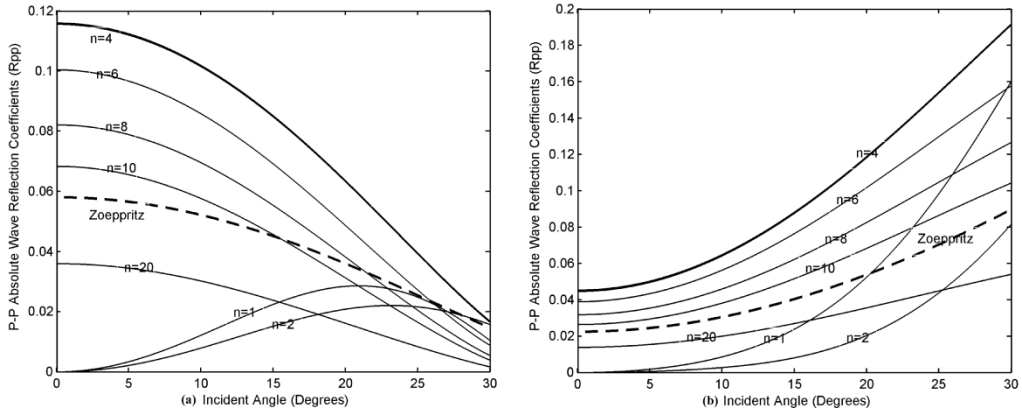

FIG.3. P-P Wave absolute reflection coefficients spectrum (frequency=30Hz) for different $n = \lambda/d$ from 1 to 20 for Model I with water sand (a) and gas sand (b) at small angles. The dashed line is calculated by Zoeppritz equation and other lines are calculated by three-layer media equation.

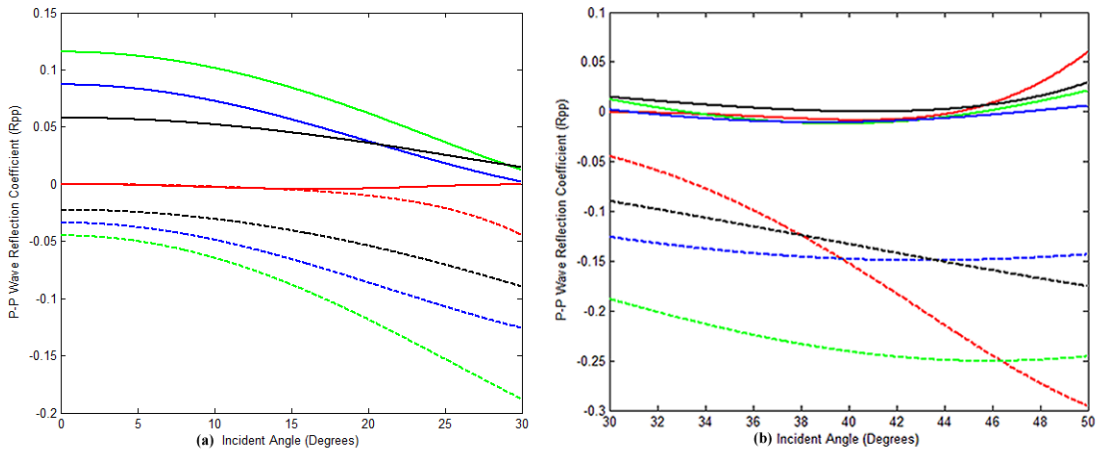

FIG.4. P-P Wave reflection coefficients spectrum at small angles (a) and middle angles (b). The dashed lines are obtained when Layer 2 is gas sand and the solid lines are obtained when Layer 2 is water sand. The different colors represent different methods or different$n = \lambda/d$. (n=2, red lines; n=4, green lines; n=6, blue lines; Zoeppritz equation, black lines)

Figure 4(a) shows the reflection coefficients at small incidence (from 0° to 30°). The solid and dashed lines are obtained when Layer 2 is water sand and gas sand respectively. The blue lines, green lines, red lines and black lines are obtained when n=2, 4, 6 and using Zoeppritz equation. Some interesting things can be found through the comparison between Figure 4(a) and Figure 4(b). At small incidence, for water sand, the polarities are positive whereas the polarities become negative when replacing the fluid with gas sand in Layer 2. This "phase conversion" can help us to recognize the occurrence of gas. What's more, when n=6, the absolute reflection coefficients are almost a constant (zero) and then gradually increase which is quite different from the AVO curves by Zoeppritz equation. At middle incidence (from 35° to 45°), for water sand the reflection coefficients calculated by three-layer media equation become negative, whereas reflection coefficients calculated by Zoeppritz equation is still positive. This means that at middle incidence when replacing the water sand with gas sand, the "Phase Conversion" changes to "Bright Spot" which can also be used to indicate gas accumulation. Zoeppritz equation is not precise and quantitative enough to found these changes and differences which are very important in fine analysis of reservoir prediction.

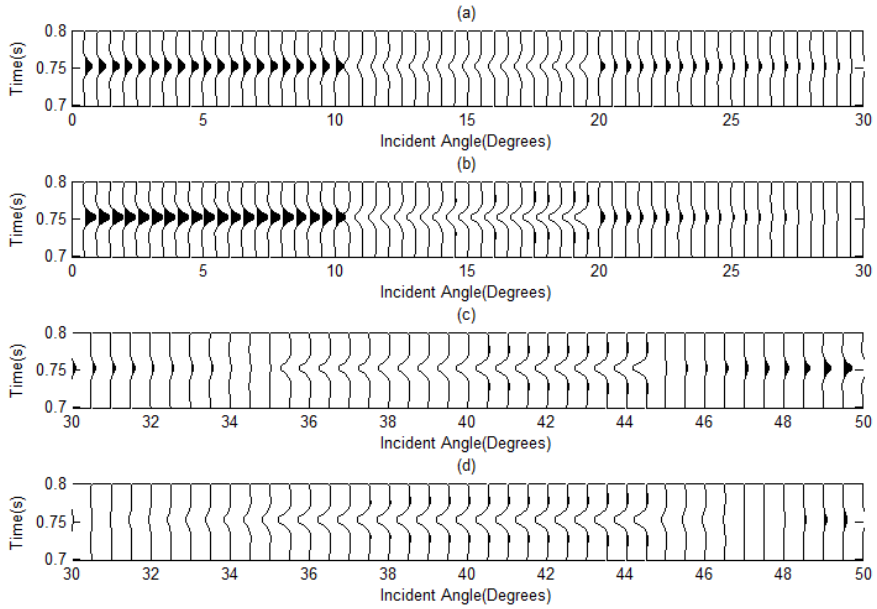

FIG.5. Four NMO corrected gathers showing amplitude anomalies for Model I. (a) "Phase Conversion" anomaly after fluids replacement at small incidence calculated by Zoeppritz equation. (b) "Phase conversion" anomaly after fluids replacement at small incidence calculated by Three-layer media equation.(c) "Phase conversion" anomaly after fluids replacement at middle incidence calculated by Zoeppritz equation. (d) "Bright Spot" anomaly after fluids replacement at middle incidence calculated by Three-layer media equation.

Figure 5 are four reflection events after NMO showing amplitude anomalies when replacing water sand with gas sand in Layer 2 calculated by Zoeppritz equation and Three-layer media equation respectively. For Figure 5(a) and (b) at small incidence, two anomalies are all "Phase Conversion". For Figure 5(c) at middle incidence, the amplitude anomaly after fluids replacement obtained by Zoeppritz equation is also "Phase Conversion". While for Figure 5(d) at middle incidence, the amplitude anomaly indicating gas sand appearance changes to "Bright Spot". This difference testifies the analysis of Figure 4 further.

Figure 6 shows the variation of absolute reflection coefficients with varying $d/\lambda = 1/n$ from 0 to 1 at different incident angles (0,10,15,20,30,40,50 degree) for water sand (a) and gas sand (b) in Layer 2. We can see that for$1/n = 0.5$, when incident angle is zero, the reflection coefficient is zero, whereas for$1/n = 0.25$, the reflection coefficient receive local maximum, which correspond to the conditions in Figure 3. What's more, it also can be noted that the two dashed lines (normal incidence) are centro-symmetric on $1/n = 0.5$ within the domain of [0, 1]. For water sand (a), when $1/n$ (from 0 to 0.25) is fixed, the absolute reflection coefficients decrease with increasing the incident angle generally. While for gas sand (b), when $1/n$ (from 0 to 0.25) is fixed, the absolute reflection coefficients increase with increasing the incident angle generally.

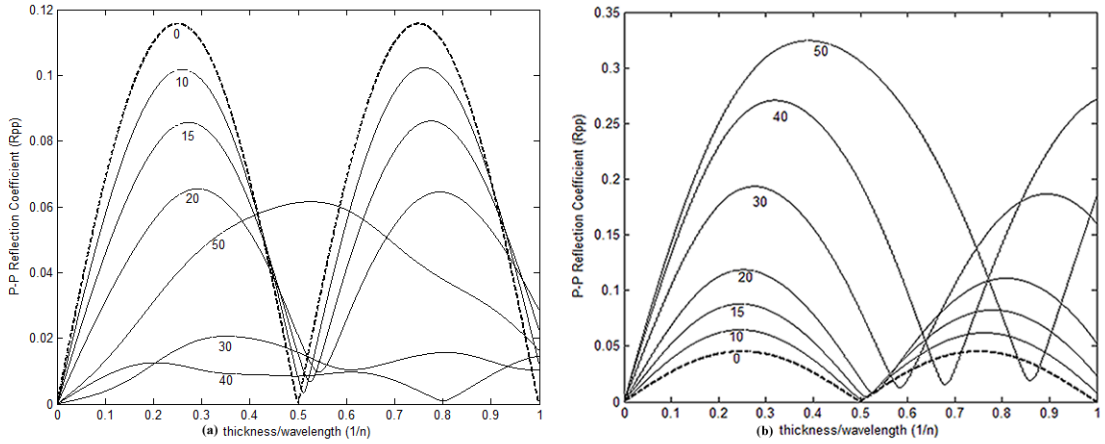

FIG.6. P-P Wave absolute reflection coefficients versus $d/\lambda = 1/n$ for water sand (a) and gas sand (b) in Layer 2 at different incident angles (0, 10, 15, 20,30,40,50 degree) The dashed lines are at normal incidence.

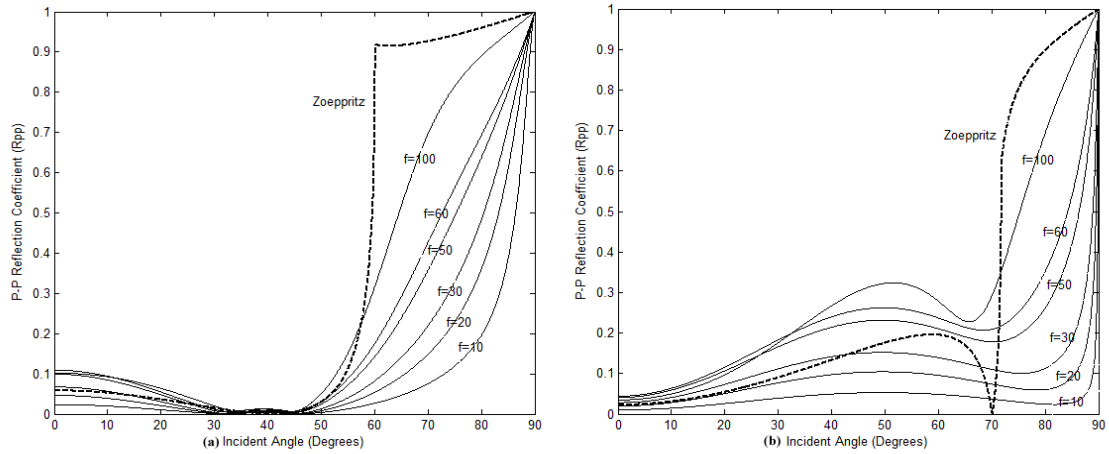

FIG.7. P-P Wave absolute reflection coefficients spectrum $(d = 10m)$ for different dominant frequency from 10Hz to 100Hz for Model I with water sand (a) and gas sand (b) at full angles. The dashed line is calculated by Zoeppritz equation and other lines are calculated by three-layer media equation.

From Figure 7, we can see that the variations of absolute reflection coefficients with increasing the incident angles for different dominant frequencies are quite similar to the variations of absolute reflection coefficients for different $\lambda/d = n$. The higher of the dominant frequency, the more flat the reflection coefficients curves become. This is opposite to the variations of reflection coefficients with increasing$\lambda/d = n$. We can build the cross-plot for thickness/wavelength (1/n) versus frequency at fixed incidence as shown in Figure 8. The color denotes normalized amplitudes. It helps us analyze the influences of frequency and thin-bed thickness on amplitudes more clearly. It can be seen that the cross-plot in Figure 8 (a) and (b) are all centro-symmetric on the diagonal lines (green). So, the influence of $\lambda/d = n$ increasing (or thin bed vanishing) is equal to that of dominant frequency decreasing.

This also provides us with one way to predict the thickness of thin bed. In seismic interpretation aiming at thin bed, we can record the different amplitudes with varying the dominant frequency of wavelet. When the amplitude receives the maximum value, the thickness of thin bed can be determined as $\lambda/4$ ("tuning thickness").

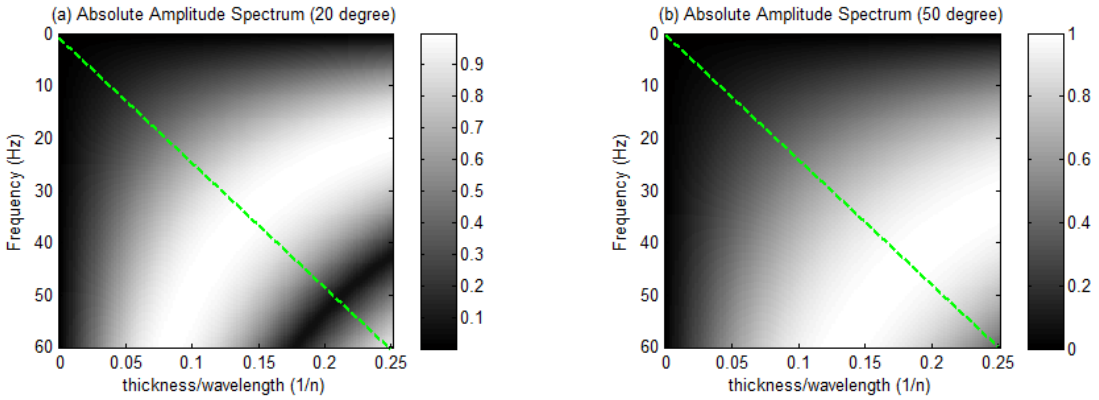

FIG.8. P-P Wave absolute amplitude spectrum with varying frequency and at fixed incident angle 20 degree (a) and 50 degree (b) for Model 1. The color represents the normalized and absolute amplitudes.

AVO responses of P-S wave (converted SV wave) with no attenuation

At oblique incidence, in elastic media, part of seismic wave energy transforms into S-wave which also contains important information of elastic parameters of the layers. V_P/V_S and Poisson's ratio σ are effective parameters for geophysicists to predict the accumulation of oil and gas. For that V_P is not only influenced by the rock framework, but also by fluids contained in the rock. When the rock pores contain oil or gas, V_S decreases apparently. Whereas V_P does not change obviously. What's more, AVO analysis of combining P-P wave and P-S wave can help us eliminate the problem of multi-solutions in hydrocarbon detection. Model II is an example to show this.

Figure 9 shows the P-P and P-S wave absolute amplitude spectrum with varying incident angle and thin bed thickness at fixed frequency (30Hz) for Model II in elastic and acoustic regimes respectively. The color represents the values of normalized amplitudes. This figure helps us analyze the variation of amplitudes with varying incident angles and thickness/wavelength $(1/n)$ more easily. Figure (a) is the P-P wave absolute amplitude spectrum for Model II with water sand in Layer 2 in elastic regime. Figure (b) is the P-P wave absolute amplitude spectrum for Model II with water sand in Layer 2 in acoustic regime. Figure (c) is the P-S wave absolute amplitude spectrum for Model II with water sand in Layer 2 in elastic regime. Figure (d), (e), and (f) are the corresponding amplitude spectrums for Model II with gas sand in Layer 2. Figure (h), (i), and (j) are the corresponding amplitude spectrums for Model II with coal in Layer 2.

It can be seen that the P-P wave amplitudes in acoustic regime (Figure (b), (e), and (i)) for different incident angles and thin bed thickness are similar to those in elastic regime (Figure (a), (d), and (h)). If we fixed thickness/wavelength at 0.25, we can extract the lines from Figure 9 and obtain the AVA curves in Figure 10. The dashed lines are calculated in elastic regime, whereas the solid lines are calculated in acoustic regime. The black, blue and green lines are for water sand (Figure (a), (b), and (c)), gas sand (Figure (d), (e), and (f)) and coal (Figure (h), (i), and (j)) in target Layer 2 respectively.

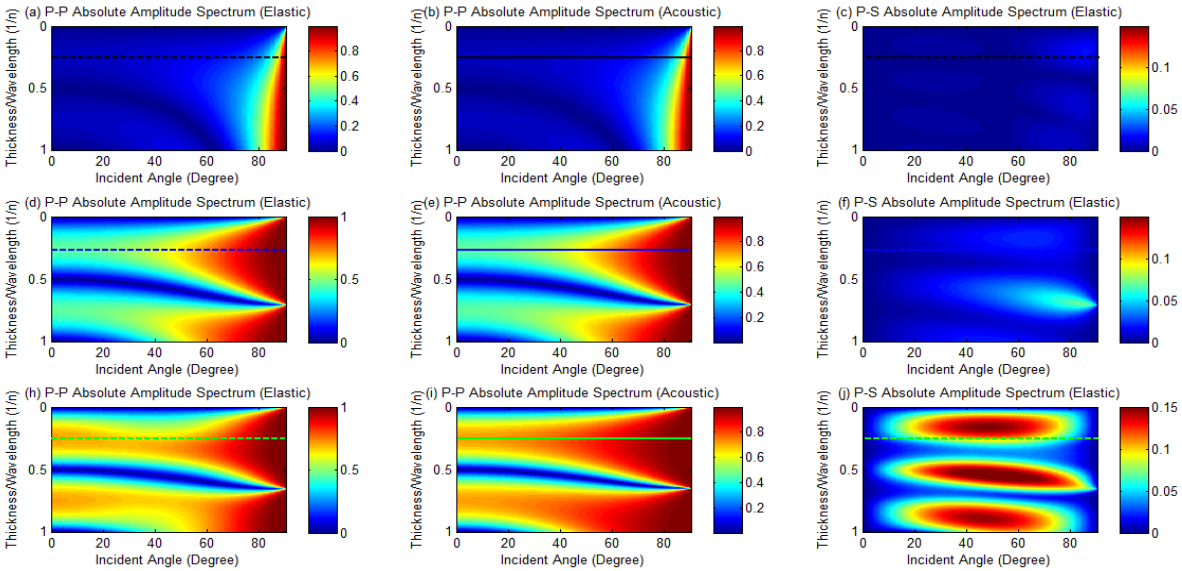

FIG.9. P-P and P-S wave absolute amplitude spectrums with varying incident angle and thickness/wavelength (1/n) at fixed frequency (30Hz) for Model II with water sand ((a), (b), (c)), gas sand ((d), (e), (f)) and coal (h), (i), (j)) in Layer 2 in elastic regime and acoustic regime respectively. The color represents normalized amplitude.

In Figure 10 (a), it is obvious that when replacing water sand in Layer 2 with gas sand or coal, the amplitude anomalies are all shown as “bright spot”. In this condition, it is difficult for us to predict the rock type in Layer 2. While if we analyze the AVA responses of P-S wave in Figure 10 (b), this problem can be settled. The differences between the amplitudes with gas sand in Layer 2 and those with water sand in Layer 2 are too small to recognize the amplitude anomaly. While amplitudes with coal in Layer 2 are quite different from those with water sand in Layer 2. The amplitude anomaly is also “bright spot” for coal.

If we increase the P-velocity of target Layer 2 and fix other elastic parameters, we can analyze the influence of P-velocity contrasts on P-S converted wave amplitudes. Figure 11 shows the P-S wave reflection coefficient curves with varying incident angle for Model I with gas sand in target Layer 2 when n=1(a), n=4(b), n=8(c) and n=10(d). We can also compare the P-S wave AVA responses by three-layer media equation (solid lines) with the P-S wave AVA responses by Zoeppritz equation (dashed lines). The color of the lines denotes different P-velocities of Layer 2 ($\alpha_2 = 2781.3, \text{black};\ \alpha_2 = 3081.3, \text{blue};\ \alpha_2 = 3381.3, \text{red}$).

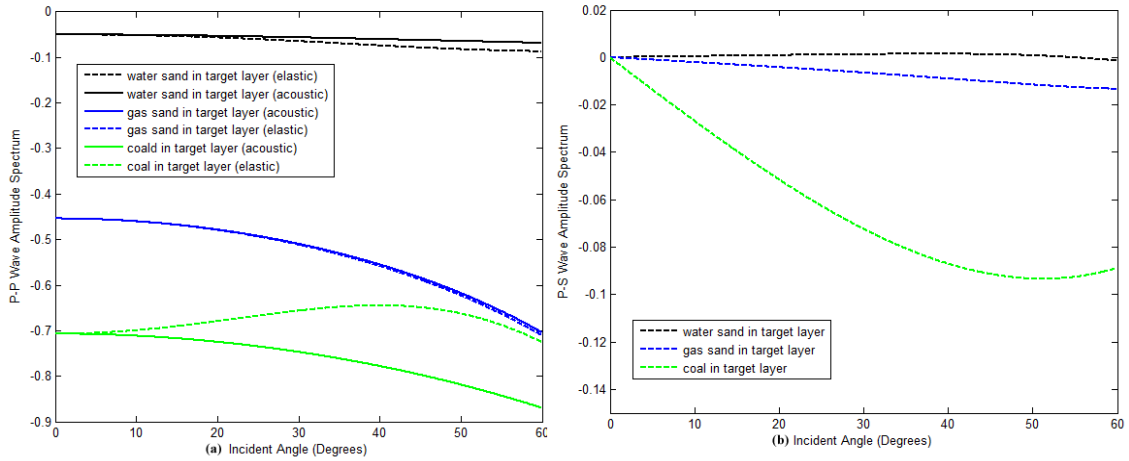

FIG.10. P-P wave (a) and P-S wave (b) amplitude spectrums with varying incident angle for fixed thin bed thickness (1/n=0.25) and fixed frequency (30Hz) for Model II. In (a), the solid and dashed lines denote the P-P wave amplitudes calculated in acoustic and elastic regime respectively. And different colors (black, blue and green) correspond to different fluids (water sand, gas sand and coal) in Layer 2. In (b), different colors (black, blue and green) correspond to different fluids (water sand, gas sand and coal) in Layer 2.

It can be seen that the P-S wave AVA responses by three-layer media equation are quite different from that by Zoeppritz equation. The polarities of the AVA curves by the two equations are opposite. What's more, with increasing the incident angle, the gradients the curves by the two equations are also different. At small incidence (0° ~30°), for n=1 (a) and n=4 (b), when increasing the P-velocity of Layer 2, the absolute reflection coefficients calculated by three-media layer equation and Zoeppritz equation all decrease. While, for n=8 (c) and n=10 (d), the differences of reflection coefficients by three-layer media equation are very small for different P-velocities of Layer 2.

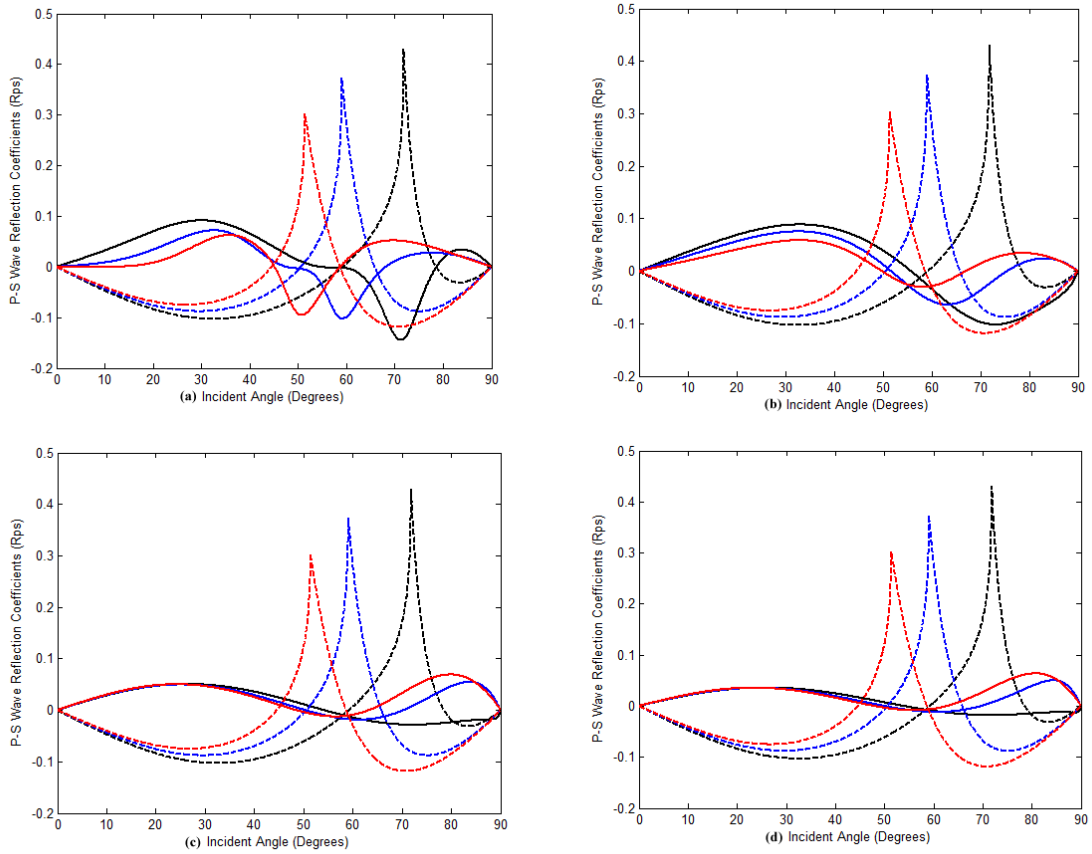

FIG.11. P-S wave reflection coefficients with varying incident angle when n=1(a), n=4(b), n=8(c) and n=10(d) for Model I with gas sand in Layer 2. The colors of the lines denote different P-velocities of Layer 2 ($\alpha_2 = 2781.3, \text{black};\ \alpha_2 = 3081.3, \text{blue};\ \alpha_2 = 3381.3, \text{red}$).

AVO RESPONSES OF THIN BED WITH ATTENUATION

If the thickness of target Layer 2 is thick enough, for instance when$n = 0.2$ and 0.1, the reflection coefficients curves calculated by three-layer media equation fluctuate and receive many local minimums and local maximums (as shown in Figure 12) with increasing the incident angle. This doesn't correspond to the practical seismic data, for that the layers absorb the energy of the reflected waves on Interface 2 which cannot receive Interface 1. This problem also exists when the incident angles are big for thin layer and ultra-thin layer ($\alpha_2 < \alpha_1$).

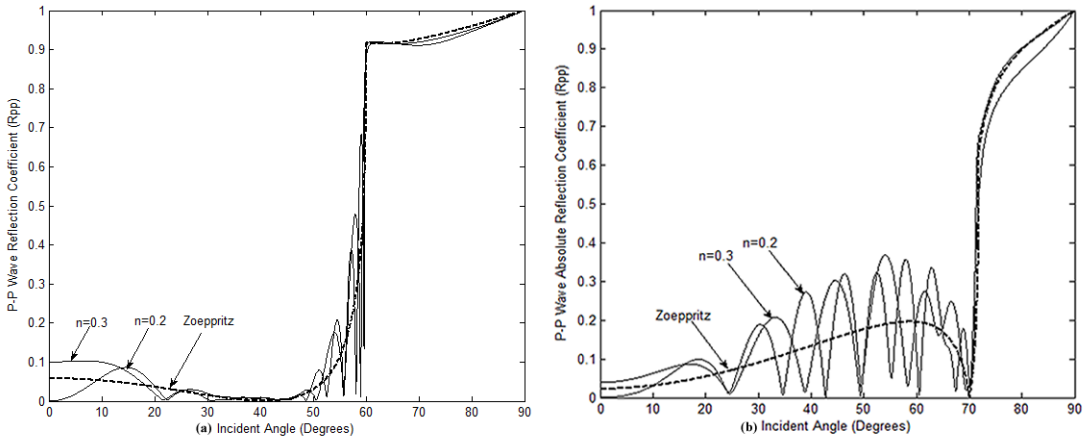

FIG.12. P-P Wave absolute reflection coefficient spectrum when $n = 0.2$ and 0.1 with water sand (a) and gas sand (b) in Layer 2 for Model I.

We can simulate the energy absorption function by setting quality factor (Q), which describes the energy change of seismic wave within one wave length (only the target Layer 2 is considered here). And then substitute equation (6) into the reflection coefficient equation. Figure 13 shows the P-P wave absolute reflection coefficients spectrum ($n = 6$) with varying quality factor Q from 5 to 100 for Model I with water sand (a) and gas sand (b) in Layer 2. The dashed line is calculated by Zoeppritz equation with no attenuation and the bold-solid line is calculated by three-layer media equation with no attenuation. In Figure 13, it is obvious that the reflection coefficients curves get closer with increasing the value of Q. It seems that decreasing Q is smoothing the curves.

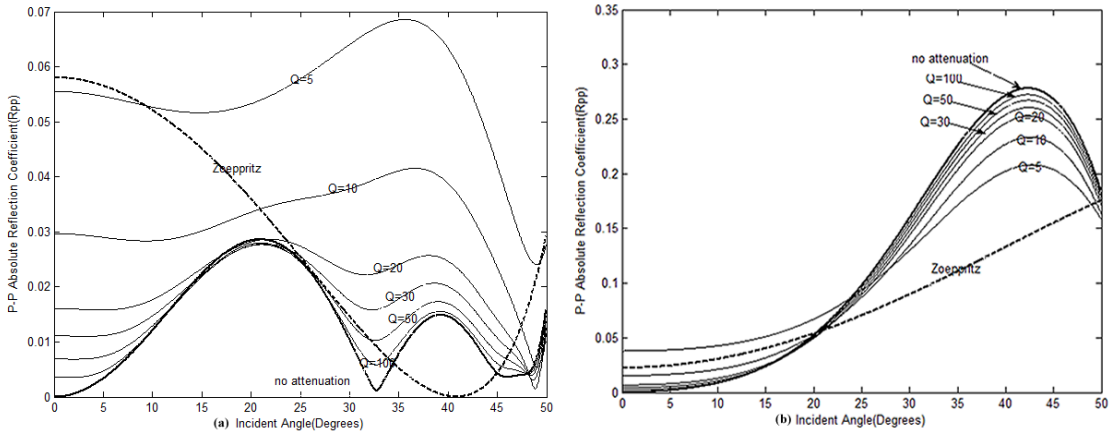

FIG.13. P-P Wave absolute reflection coefficients spectrum ($n = 6$) for different Q (5,10,20,30,50,100) for Model I with water sand (a) and gas sand (b) in Layer 2. The dashed line is calculated by Zoeppritz equation and other lines are calculated by three-layer media equation.

Assuming that the target Layer 2 has strong absorption ability and is thick enough, the reflection coefficients calculated by three-layer media equation will get close to the

reflection coefficients calculated by Zoeppritz equation with attenuation. Figure 14 testifies this prediction. The red-solid line calculated by three-layer media equation with no attenuation fluctuates seriously. While the red-dash line become smooth and get close to the black-dash line calculated by Zoeppritz equation.

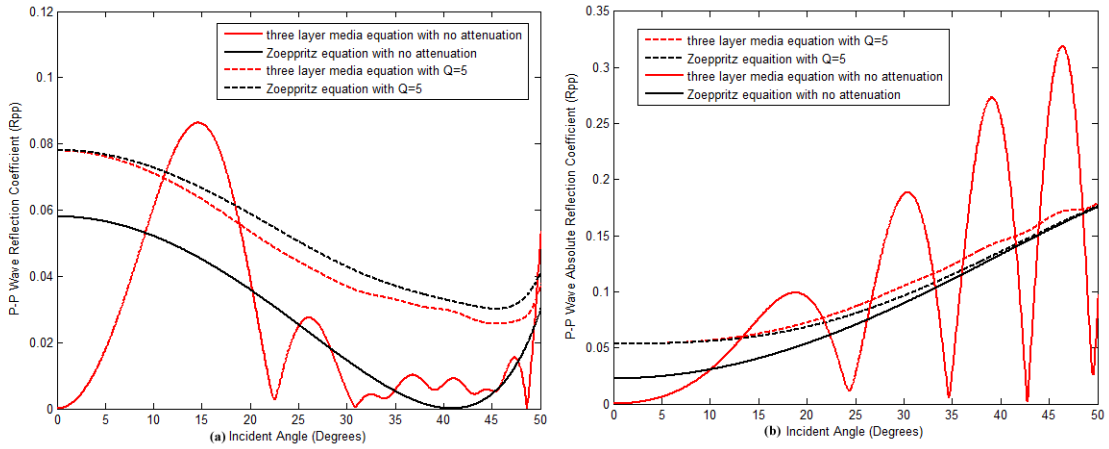

FIG.14. P-P Wave absolute reflection coefficients curves comparison (n = 0.2) for Model I with water sand (a) and gas sand (b) in Layer 2. Black-solid line is calculated by Zoeppritz equation with no attenuation; Red-solid line is calculated by three-layer media equation with no attenuation. Black-dash line is calculated by Zoeppritz equation with Q=5; Red-dash line is calculated by three-layer media equation with Q=5.

CONCLUSION

AVO technology is an effective method for exploration geophysicists to recognize oil and gas reservoir. While traditional AVO analysis is based on Zoeppritz equation which only contains the information of single interface. The three-layer media equation derived in this study describes the propagation of seismic wave in layered-media. Even though, we don't derive the direct expression of reflection coefficients or its linear approximations, this equation is still suitable to analyze the AVO responses of thin bed with varying the incident angle, frequency and thin bed thickness in elastic regime. What's more, the influences of absorption function (only target Layer 2 is considered here) for different Q is also discussed in this paper.

Several conclusions can be arrived at: (1) taking the reflections from bottom interface into consideration, the AVO/AVA responses by three-layer media equation are more precise than the AVO/AVA responses by Zoeppritz equation; (2) if the incident angle is fixed, the influence of thin bed thinning on variations of amplitudes is equal to the influence of dominant frequency decreasing; (3) the AVO responses of P-S wave, which also contains the information of rock properties, is important in fine hydrocarbon prediction ; (4) With decreasing Q (quality factor), the AVO curve calculated by three-layer media equation become more smooth and get closer to the curve calculated by Zoeppritz equation.

Because the reflection coefficients equation is too complicated to inverse directly, we can use the nonlinear optimization algorithms such as Simulated Annealing Algorithm or Genetic Algorithm. To improve the precision of the inversion results and computational efficiency, we can limit the ranges of optimal solutions and carry out some other strategies which are the next step of the research.

APPENDIX A

A plane harmonic wave illuminates the Layer 2 as shown in Figure 1.For elastic media, the displacement potential functions of P-wave and S-wave in Layer 1 and Layer 3 can be written respectively as

$$\phi_1 = A_1' \, exp[j(\sigma_1 x - \tau_1 z - \omega t)] + A_1'' exp[j(\sigma_1 x + \tau_1 z - \omega t)], \quad \text{(A-1)}$$

$$\phi_3 = A_3' exp[j(\sigma_3 x - \tau_3 z - \omega t)], \quad \text{(A-2)}$$

$$\varphi_1 = B_1' exp[j(\sigma_1' x + \tau_1' z - \omega t)], \quad \text{(A-3)}$$

$$\varphi_3 = B_3' exp[j(\sigma_3' x - \tau_3' z - \omega t)], \quad \text{(A-4)}$$

where $\sigma_i = \kappa_i \sin\theta_i$; $\tau_i = \kappa_i \cos\theta_i$; $\sigma_i' = \kappa_i' \sin\theta_i$; $\tau_i' = \kappa_i' \cos\theta_i$; $i = 1,3$; κ_i and κ_i' are the wave-numbers of P-wave and S-wave in Layer i respectively. σ_i and τ_i are the horizontal and vertical components of P wave-number respectively. σ_i' and τ_i' are the horizontal and vertical components of S wave-number respectively. θ_i represents the incident or refracted angles as shown in Figure 1. A_i' and B_i' refer to the amplitudes of P-wave and S-wave respectively. ω is the angular frequency. It is known that

$$\sigma_1 = \frac{\omega}{\alpha_1} \sin\theta_1, \quad \text{(A-5)}$$

where α_1 is P-wave velocity in Layer 1. And

$$\sigma_1' = \frac{\omega}{\beta_1} \sin\gamma_1, \quad \text{(A-6)}$$

where γ_1 and β_1 are the reflection angle and velocity of S-wave in Layer 1. Then

$$\sigma_1' = \frac{\omega}{\alpha_1}\frac{\alpha_1}{\beta_1} \sin\gamma_1 = \frac{\omega}{\alpha_1}\frac{\sin\theta_1}{\sin\gamma_1} \sin\gamma_1 = \sigma_1, \quad \text{(A-7)}$$

So we can set

$$\sigma = \sigma_1 = \sigma_1' = \sigma_3 = \sigma_3', \quad \text{(A-8)}$$

equations (A-1) -(A-5) can be written as

$$\phi_1 = A_1' \, exp[j(\sigma x - \tau_1 z - \omega t)] + A_1'' exp[j(\sigma x + \tau_1 z - \omega t)], \quad \text{(A-9)}$$

$$\phi_3 = A_3' exp[j(\sigma x - \tau_3 z - \omega t)], \quad \text{(A-10)}$$

$$\varphi_1 = B_1' ex\, p[j(\sigma x + \tau_1' z - \omega t)], \quad \text{(A-11)}$$

$$\varphi_3 = B_3' ex\, p[j(\sigma x - \tau_3' z - \omega t)] \,, \quad \text{(A-12)}$$

u and v represent the displacements in X direction and Z direction respectively. And they can be written as

$$\begin{aligned} u &= \left(\frac{\partial \phi}{\partial x} - \frac{\partial \varphi}{\partial z}\right) \\ v &= \left(\frac{\partial \phi}{\partial z} + \frac{\partial \varphi}{\partial x}\right) \end{aligned}, \quad \text{(A-13)}$$

And the stress in X direction and Z direction are σ_{zz} and τ_{zx}.

$$\begin{aligned} \sigma_{zz} &= \lambda \left(\frac{\partial u}{\partial x} + \frac{\partial v}{\partial z}\right) + 2\mu \frac{\partial v}{\partial z} \\ \tau_{zx} &= \mu \left(\frac{\partial v}{\partial x} + \frac{\partial u}{\partial z}\right) \end{aligned}, \quad \text{(A-14)}$$

where λ is lame coefficient and μ is shear modulus.

Substituting equations (A-9) and (A-11) into equation (A-13) and then into equation (A-14). We can obtain the displacements and stress in Layer 1 which are

$${u_x}^1 = \left[j\sigma\left(A_1' e^{-j\tau_1 z} + A_1'' e^{j\tau_1 z}\right) - j\tau_1' B_1' e^{j\tau_1' z}\right] e^{j(\sigma x - \omega t)}, \quad \text{(A-15)}$$

$${v_z}^1 = \left[-j\tau_1\left(A_1' e^{-j\tau_1 z} - A_1'' e^{j\tau_1 z}\right) + j\sigma B_1' e^{j\tau_1' z}\right] e^{j(\sigma x - \omega t)}, \quad \text{(A-16)}$$

$${\sigma_{zz}}^1 = -\left[(\lambda_1 \kappa_1^2 + 2\mu_1 \tau_1^2)\left(A_1' e^{-j\tau_1 z} + A_1'' e^{j\tau_1 z}\right) + 2\mu_1 \sigma \tau_1' B_1' e^{j\tau_1' z}\right] e^{j(\sigma x - \omega t)}, \quad \text{(A-17)}$$

$${\tau_{zx}}^1 = \mu_1\left[2\tau_1 \sigma\left(A_1' e^{-j\tau_1 z} - A_1'' e^{j\tau_1 z}\right) + \left({\tau_1'}^2 - \sigma^2\right) B_1' e^{j\tau_1' z}\right] e^{j(\sigma x - \omega t)}, \quad \text{(A-18)}$$

According to Maclaurin's rule

$$e^{j\tau_1 z} = \cos(j\tau_1 z) + j\sin(\tau_1 z) = \ \cosH + j\sinH, \quad \text{(A-19)}$$

$$e^{-j\tau_1 z} = \cos(-j\tau_1 z) - j\sin(\tau_1 z) = \ \cosH - j\sinH, \quad \text{(A-20)}$$

$$e^{j\tau_1' z} = \cos(j\tau_1' z) + j\sin(\tau_1' z) = \ \cosR + j\sinR, \quad \text{(A-21)}$$

$$e^{-j\tau_1' z} = \cos(-j\tau_1' z) - j\sin(\tau_1' z) = \ \cosR - j\sinR, \quad \text{(A-22)}$$

where $H = \tau_1 z = \frac{\omega}{\alpha_1} \cos\theta_1 z$ and $R = \tau_1' z = \frac{\omega}{\beta_1} \cos\gamma_1 z$. And on the bottom interface of Layer 1 where $z = 0$, so the displacements are

$$u_x{}^1 = [j\sigma(A_1' + A_1'') - j\tau_1' B_1']e^{j(\sigma x - \omega t)}, \quad \text{(A-23)}$$

$$v_z{}^1 = [-j\tau_1(A_1' - A_1'') + j\sigma B_1']e^{j(\sigma x - \omega t)}, \quad \text{(A-24)}$$

$$\sigma_{zz}{}^1 = -[(\lambda_1\kappa_1^2 + 2\mu_1\tau_1^2)(A_1' + A_1'') + 2\mu_1\sigma\tau_1' B_1']e^{j(\sigma x - \omega t)}, \quad \text{(A-25)}$$

$$\tau_{zx}{}^1 = \mu_1\left[2\tau_1\sigma(A_1' - A_1'') + \left(\tau_1'{}^2 - \sigma^2\right)B_1'\right]e^{j(\sigma x - \omega t)}, \quad \text{(A-26)}$$

Then we get

$$\begin{bmatrix} u_x{}^1 \\ v_z{}^1 \\ \sigma_{zz}{}^1 \\ \tau_{zx}{}^1 \end{bmatrix} = \begin{bmatrix} j\sigma & 0 & -j\tau_1' & 0 \\ 0 & -j\tau_1 & 0 & j\sigma \\ -(\lambda_1\kappa_1^2 + 2\mu_1\tau_1^2) & 0 & -2\mu_1\sigma\tau_1' & 0 \\ 0 & 2\mu_1\tau_1\sigma & 0 & \tau_1'{}^2 - \sigma^2 \end{bmatrix} \begin{bmatrix} A_1' + A_1'' \\ A_1' - A_1'' \\ B_1' \\ B_1' \end{bmatrix} e^{j(\sigma x - \omega t)}, \quad \text{(A-27)}$$

and

$$\begin{bmatrix} A_1' + A_1'' \\ A_1' - A_1'' \\ B_1' \\ B_1' \end{bmatrix} e^{j(\sigma x - \omega t)} = \begin{bmatrix} j\sigma & 0 & -j\tau_1' & 0 \\ 0 & -j\tau_1 & 0 & j\sigma \\ -(\lambda_1\kappa_1^2 + 2\mu_1\tau_1^2) & 0 & -2\mu_1\sigma\tau_1' & 0 \\ 0 & 2\mu_1\tau_1\sigma & 0 & \tau_1'{}^2 - \sigma^2 \end{bmatrix}^{-1} \begin{bmatrix} u_x{}^1 \\ v_z{}^1 \\ \sigma_{zz}{}^1 \\ \tau_{zx}{}^1 \end{bmatrix}, \quad \text{(A-28)}$$

Similarly, we can obtain the displacement and stress on the bottom interface of Layer 2 where $z = d$, d is the thickness of Layer 2.

$$\begin{bmatrix} u_x{}^2 \\ v_z{}^2 \\ \sigma_{zz}{}^2 \\ \tau_{zx}{}^2 \end{bmatrix} = \begin{bmatrix} j\sigma\cos H & \sigma\sin H & -j\tau_2'\cos R & j\tau_2'\sin R \\ -\tau_2\sin H & j\tau_2\cos H & -\sigma\sin R & j\sigma\cos R \\ -(\lambda_2\kappa_2^2 + 2\mu_2\tau_2^2)\cos H & -(\lambda_2\kappa_2^2 + 2\mu_2\tau_2^2)\sin H & -2\mu_2\sigma\tau_2'\cos R & 2\mu_2\sigma\tau_2'\sin R \\ 2\mu_2\tau_2\sigma\sin H & 2\mu_2\tau_2\sigma\cos H & \left(\tau_2'{}^2 - \sigma^2\right)\cos R & \left(\tau_2'{}^2 - \sigma^2\right)\sin R \end{bmatrix}$$
$$\times \begin{bmatrix} A_1' + A_1'' \\ A_1' - A_1'' \\ B_1' \\ B_1' \end{bmatrix} e^{j(\sigma x - \omega t)}, \quad \text{(A-29)}$$

Set

$$\mathrm{M} = \begin{bmatrix} j\sigma & 0 & -j\tau_1' & 0 \\ 0 & -j\tau_1 & 0 & j\sigma \\ -(\lambda_1\kappa_1^2 + 2\mu_1\tau_1^2) & 0 & -2\mu_1\sigma\tau_1' & 0 \\ 0 & 2\mu_1\tau_1\sigma & 0 & \tau_1'{}^2 - \sigma^2 \end{bmatrix}^{-1}, \quad \text{(A-30)}$$

$$N=\begin{bmatrix} j\sigma\cos H & \sigma\sin H & -j\tau_2'\cos R & j\tau_2'\sin R \\ -\tau_2\sin H & j\tau_2\cos H & -\sigma\sin R & j\sigma\cos R \\ -\left(\lambda_2\kappa_2^2+2\mu_2\tau_2^2\right)\cos H & -\left(\lambda_2\kappa_2^2+2\mu_2\tau_2^2\right)\sin H & -2\mu_2\sigma\tau_2'\cos R & 2\mu_2\sigma\tau_2'\sin R \\ 2\mu_2\tau_2\sigma\sin H & 2\mu_2\tau_2\sigma\cos H & \left(\tau_2'^{\,2}-\sigma^2\right)\cos R & \left(\tau_2'^{\,2}-\sigma^2\right)\sin R \end{bmatrix}, \quad \text{(A-31)}$$

Then

$$\begin{bmatrix} u_x{}^2 \\ v_z{}^2 \\ \sigma_{zz}{}^2 \\ \tau_{zx}{}^2 \end{bmatrix} = \mathrm{NM}\begin{bmatrix} u_x{}^1 \\ v_z{}^1 \\ \sigma_{zz}{}^1 \\ \tau_{zx}{}^1 \end{bmatrix}, \quad \text{(A-32)}$$

Because the displacement and stress on the Interface 2 are continuous, the displacement and stress on the top interface of Layer 3 are equal to those of bottom interface of Layer 2. So

$$\begin{bmatrix} u_x{}^3 \\ v_z{}^3 \\ \sigma_{zz}{}^3 \\ \tau_{zx}{}^3 \end{bmatrix} = \begin{bmatrix} u_x{}^2 \\ v_z{}^2 \\ \sigma_{zz}{}^2 \\ \tau_{zx}{}^2 \end{bmatrix} = \mathrm{NM}\begin{bmatrix} u_x{}^1 \\ v_z{}^1 \\ \sigma_{zz}{}^1 \\ \tau_{zx}{}^1 \end{bmatrix}, \quad \text{(A-33)}$$

And

$$\mathrm{C}=\mathrm{NM}=\begin{bmatrix} c_{11} & c_{12} & c_{13} & c_{14} \\ c_{21} & c_{22} & c_{23} & c_{24} \\ c_{31} & c_{32} & c_{33} & c_{34} \\ c_{41} & c_{42} & c_{34} & c_{44} \end{bmatrix}, \quad \text{(A-34)}$$

Where

$c_{11}=2sin^2\gamma_2 cosH+cos2\gamma_2 cosR$, $c_{12}=j(tan\theta_2 cos2\gamma_2 sinH-sin2\gamma_2 sinR)$,

$c_{13}=\dfrac{sin\theta_2}{\rho_2\alpha_2}(cosR-cosH)$

$c_{14}=-2j\beta_2(tan\theta_2 sin\gamma_2 sinH+cos\gamma_2 sinR)$,

$$c_{21} = j(\frac{\beta_2 cos\theta_2}{\alpha_2 cos\gamma_2} sin2\gamma_2 sinH - tan\gamma_2 cos2\gamma_2 \gamma sinR)$$
$$c_{22} = cos2\gamma_2 cos2H - 2sin^2 cosR$$
$$c_{23} = -\frac{j}{\rho_2 \alpha_2}(cos\theta_2 sinH - tan\gamma_2 sin\theta_2 sinR)$$
$$c_{24} = 2\beta_2 sin\gamma_2(cosR - cosH) \quad c_{31} = -2\rho_2 \beta_2 sin\gamma cos2\gamma_2(cosR - cosH)$$
$$c_{32} = -j\rho_2(\frac{\alpha_2 cos^2 2\gamma_2}{cos\theta_2} sinH + 4\beta_2 cos\gamma_2 sin^2\gamma_2 sinR)$$
$$c_{33} = cos2\gamma_2 cosH cosR + 2sin^2\gamma_2 cosR)$$
$$c_{34} = -2j\rho_2(cos2\gamma_2 tan\theta_2 sinH + sin2\gamma_2 sinR)$$
$$c_{41} = j(\frac{2}{\alpha_2} cos\theta_2 sin^2\gamma_2 sinH + \frac{cos^2 2\gamma_2}{2V_s cos\gamma_2} sinR$$
$$c_{42} = \frac{sin\theta_2 cos2\gamma_2}{\alpha_2}(cosR - cosH)$$
$$c_{43} = -\frac{j}{2\rho_2}(\frac{sin2\theta_2}{\alpha_2^2} sinH - \frac{cos2\gamma_2}{\beta_2^2} tan\gamma_2 sinR)$$
$$c_{44} = 2sin^2\gamma_2 cosH + cos2\gamma_2 cosR$$

where α_2, β_2, θ_2, γ_2, ρ_2 are the P-wave velocity, S-wave velocity, transmission angle of P-wave, transmission angle of S-wave, and density within Layer 2. And $H = \frac{\omega}{\alpha_2} cos\theta_2 z$, $R = \frac{\omega}{\beta_2} cos\gamma_2 z$. So, we call equation (A-33) as three-layer equation.

Substituting equation (A-27) and (A-29) into equation (A-33), we have

$$\begin{bmatrix} j\sigma T_{pp} + j\tau_3' T_{ps} \\ -j\tau_3 T_{pp} + j\sigma T_{ps} \\ -\left[(\lambda_3\kappa_3^2 + 2\mu_3\tau_3^2)T_{pp} - 2\mu_3\sigma\tau_3' T_{ps}\right] \\ \mu_3\left[2\tau_1\sigma T_{pp} + \left(\tau_1'^2 - \sigma^2\right)T_{ps}\right] \end{bmatrix} = C \begin{bmatrix} j\sigma(R_{pp} + 1) + j\tau_1' R_{ps} \\ j\tau_1(R_{pp} - 1) + j\sigma R_{ps} \\ -\left[(\lambda_1\kappa_1^2 + 2\mu_1\tau_1^2)(R_{pp} + 1) + 2\mu_1\sigma\tau_1' R_{ps}\right] \\ -\mu_1\left[2\tau_1\sigma(R_{pp} - 1) + \left(-\tau_1'^2 + \sigma^2\right)R_{ps}\right] \end{bmatrix}, \quad \text{(A-35)}$$

where $R_{pp} = \frac{A_1''}{A_1'}$, $R_{ps} = \frac{B_1'}{A_1'}$, $T_{pp} = \frac{A_3'}{A_1'}$, $T_{ps} = \frac{B_3'}{A_1'}$ are reflection coefficients and transmission coefficients of P-wave and S-wave respectively. According to the models used, the elastic parameters of Layer 1 are equal to those of Layer 3, then

$$\begin{bmatrix} v_{11} & v_{12} & v_{13} & v_{14} \\ v_{21} & v_{22} & v_{23} & v_{24} \\ v_{31} & v_{32} & v_{33} & v_{34} \\ v_{41} & v_{42} & v_{43} & v_{44} \end{bmatrix} \begin{bmatrix} R_{pp} \\ R_{ps} \\ T_{pp} \\ T_{ps} \end{bmatrix} = \begin{bmatrix} x_1 \\ x_2 \\ x_3 \\ x_4 \end{bmatrix}, \quad \text{(A-36)}$$

where

$$\begin{bmatrix} v_{11} \\ v_{21} \\ v_{31} \\ v_{41} \end{bmatrix} = \mathrm{C}\begin{bmatrix} sin\theta_1 \\ cos\theta_1 \\ -Z_1 cos2\gamma_1 \\ -\frac{\mu_1 sin2\theta_1}{2\mu_2\alpha_1} \end{bmatrix}, \quad \begin{bmatrix} v_{12} \\ v_{22} \\ v_{32} \\ v_{42} \end{bmatrix} = \mathrm{C}\begin{bmatrix} -\frac{sin\theta_1}{sin\gamma_1}cos\gamma_1 \\ sin\theta_1 \\ Z_1 sin2\gamma_1 \\ -\frac{Z_1}{2\mu_2}cos2\gamma_1 \end{bmatrix}, \quad \begin{bmatrix} v_{13} \\ v_{23} \\ v_{33} \\ v_{43} \end{bmatrix} = \begin{bmatrix} -sin\theta_1 \\ cos\theta_1 \\ Z_1 cos2\gamma_1 \\ -\frac{\mu_1 sin2\theta_1}{2\mu_2\alpha_1} \end{bmatrix},$$

$$\begin{bmatrix} v_{14} \\ v_{24} \\ v_{34} \\ v_{44} \end{bmatrix} = \begin{bmatrix} -\frac{sin\theta_1}{sin\gamma_1}cos\gamma_1 \\ -sin\theta_1 \\ -Z_1 sin2\gamma_1 \\ -\frac{Z_1}{2\mu_2}cos2\gamma_1 \end{bmatrix}, \begin{bmatrix} x_1 \\ x_2 \\ x_3 \\ x_4 \end{bmatrix} = \mathrm{C}\begin{bmatrix} -sin\theta_1 \\ cos\theta_1 \\ Z_1 cos2\gamma_1 \\ -\frac{\mu_1 sin2\theta_1}{2\mu_2\alpha_1} \end{bmatrix}, V = \begin{bmatrix} v_{11} & v_{12} & v_{13} & v_{14} \\ v_{21} & v_{22} & v_{23} & v_{24} \\ v_{31} & v_{32} & v_{33} & v_{34} \\ v_{41} & v_{42} & v_{43} & v_{44} \end{bmatrix}, X = \begin{bmatrix} x_1 \\ x_2 \\ x_3 \\ x_4 \end{bmatrix},$$

$\mathrm{Z}_1 = \rho_1\alpha_1$.

According to Cramer's rule, we can obtain four matrices V_{pp}, V_{ps}, V'_{pp} and V'_{ps} by replacing the first, the second, the third and then the fourth columns of matrix V with X. Then we can the reflection and transmission coefficients

$$R_{pp} = \frac{\det V_{pp}}{\det V}, R_{ps} = \frac{\det V_{ps}}{\det V}, T_{pp} = \frac{\det V'_{pp}}{\det V}, T_{ps} = \frac{\det V'_{ps}}{\det V}, \qquad \text{(A-37)}$$

Where $\det V_{pp}$, $\det V_{ps}$, $\det V'_{pp}$, $\det V'_{ps}$, and $\det V$ are the determinants of the matrices.

When the incident angle is zero (normal incidence), we can get

$$R_{pp} = \frac{-j\left(\frac{Z_1^2}{Z_2} - Z_2\right)sinH}{2Z_1 cosH + j\left(\frac{Z_1^2}{Z_2} + Z_2\right)sinH}, \qquad \text{(A-38)}$$

$$T_{pp} = \frac{1}{Z_1}\left[(Z_1 cosH + jZ_2 sinH)\frac{-j\left(\frac{Z_1^2}{Z_2} - Z_2\right)sinH}{2Z_1 cosH + j\left(\frac{Z_1^2}{Z_2} + Z_2\right)sinH} + (Z_1 cosH - jZ_2 sinH)\right], \qquad \text{(A-39)}$$

$$R_{ps} = T_{ps} = 0, \qquad \text{(A-40)}$$

ACKNOWLEDGEMENT

The sponsors of CREWES and Kris Innanen are gratefully acknowledged for their support of this research.

REFERENCES

Aki, K., and Richards, P.G., 1980. Quantitative seismology: Theory and methods, Vol. 1: W.H. Freeman & Co., San Francisco, CA.

Ball V. 1988. Thin bed tuning analysis using AVO stratigraphy methods. 58th SEG meeting, Anaheim, USA, Expanded Abstracts, 1213–1216.

Brekhovski, LM, Translated by Yang, XR, 1960. Wave in layered media: Science Press (in Chinese).

Chung, H. M., and Lawton, D. C., 1995. Amplitude responses of thin beds: Sinusoidal approximation versus Ricker approximation: Geophysics, **60**, 223–230.

Fryaer, G.J., 1978, Reflectivity of the ocean bottom at lower frequency J. Acous. Soc. Am 63(l).

Gidlow, P. M., Smith, G. C., and Vail, P. J., 1992. Hydrocarbon detection using fluid factor traces: Joint SEG /EAGE Summer Research Workshop, Technical Program and Abstracts, 78–89.

Hilterman, F. J., 2001. Seismic amplitude interpretation, SEG.

Juhlin, C., and Young, R., 1993. Implications of thin layers for amplitude variation with offset (AVO) studies: Geophysics, **58**, 1200-1204.

Koefoed, O., 1955. On the effect of Poisson's ratios of rock strata on the reflection coefficients of plane waves: Geophysical Prospecting, **3**, 381–387.

Innanen, K. A., 2011. AVO analysis of P-, S-, and C-wave elastic and anelastic reflection data. CREWES Research Report.

Shuey, R. T., 1985. A simplification of the Zoeppritz equations: Geophysics, **50**, 609–614.

Swan H. 1988. Amplitude versus offset analysis in a finely layered media. 58th SEG meeting, Anaheim, USA, Expanded Abstracts, 1195–1198.

Yinbin, L and Douglas R. S., 2003. Amplitude and AVO responses of a single thin bed: Geophysics, **68**, 1161-1168.

Widess, M.B., 1973. How thin is a thin bed?: Geophysics, **38**, 1176–1180.